Electron spectroscopies and their use for materials characterization

Didier SÉBILLEAU[1], Zi-Yu WU[2]

([1]Laboratoire PALMS, UMR CNRS-Université 6627, Bât. 11C, Université de Rennes-1, 35042 Rennes-Cédex, France;

[2]Beijing Synchrotron Radiation Facility, Institute of High Energy Physics, the Chinese Academy of Sciences, Beijing 100039, China)

Abstract We present here a general overview of electron spectroscopies from a practical point of view. The most frequently used ones are described and the type of structural information they can provide on materials is explained in relation to the physical processes on which they are based. Furthermore, we explore critically and in detail various tools that have been developed to allow a systematic solving of structures by these spectroscopies.

Keywords Electron spectroscopy, Materials characterization, Surface analysis

CLC numbers O657.62, O766

1 Introduction

Electron spectroscopies are among all the techniques to characterize materials and their surfaces some of the most accurate that are currently available.[1] Since the starting of Low-Energy Electron Diffraction (LEED) as a surface crystallographic tool in the late 1960's, many other such electron spectroscopies have been devised using the same basic processes to study from a microscopic point of view both the surface and bulk properties of materials. They form now a set of powerful and versatile tools, often complementary as no single technique can give all the information by itself, that are quite unavoidable to study materials. These techniques generally follow the same procedure : a spectrum, characteristic of the spectroscopy is recorded and then, features of this spectrum, such as its maximum or its area, are monitored as a function of the energy or the direction of the signal detected, or of the incident signal, or as a function of any potential that can be applied to the system.

In our view, the term "electron spectroscopy" means literally that the features in the spectra measured in the experiment are due to the multiple scattering of electrons by neighboring atoms. This does not preclude of the type of particle entering the detector. In particular, we consider X-ray Absorption Spectroscopy (XAS) as an electron spectroscopy although it is photons that are detected, because the signal measured by the detector is largely due to the scattering of the electrons excited by the absorbed photons. Hence, XAS is much closer to LEED or Photoelectron Diffraction (PhD) than to diffraction techniques such as X-ray Diffraction (XRD) or X-ray Standing Waves (XSW). Consequently, the term "electron spectroscopy" must be understood as describing any technique where the information that will have to be extracted from the experimental data has been gathered by electrons whether these electrons are ultimately detected or not. This is sketched in Fig.1 where only electrons and photons have been represented for the incoming and the outgoing beam, although other cases are possible.

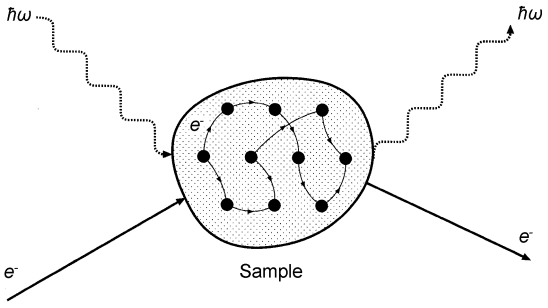

Fig.1 A schematic of electron spectroscopies. Here, the information is gathered by an electron in the sample. Only electrons and photons are represented as possible incoming and outgoing particles but other ones such as ions or atoms can be used as long as their effect is to excite an electron that will probe the sample.

The type of information that can be obtained from these techniques largely depends on the length scale of

Zi-Yu WU: E-mail: wuzy@ihep.ac.cn

Received date: 2002-11-25

interest. As it has been discussed in details by Van Hove,[2] these spectroscopies can cover mainly three types of scales : mesoscopic, nanoscopic and atomic. For the mesoscale, they can provide accurate information on morphology, islands type, size and formation, domains or boundaries and more generally on any type of defects and disorder, and on the chemical composition. In this case, only qualitative information is usually needed and hence, no substantial theoretical analysis is necessary. This information can be obtained from the spectra without making use of sophisticated and tedious calculations. Photoemission using either UV (UPS) or X-ray (XPS) radiations, together with Scanning Tunneling Microscopy (STM), Auger Electron Spectroscopy (AES) and LEED are here among the most informative techniques in this length scale. At the other end of the scale, on the atomic scale, for which most of these techniques have been devised and perfected along the years, the interest lies in properties sensitive to the crystalline structure on the order of a hundredth of a nanometer or even less. The type of information that can be extracted here ranges from crystallographic structure to electronic or magnetic structure. Crystallographic information is obtained by using probe electrons of sufficiently high kinetic energy to allow them to escape the sample. On the contrary, when this energy is small, they will rather populate the empty states in the sample than escape, and therefore give information on the electronic structure. The introduction of chirality in the system, either by studying magnetic materials and reversing an applied magnetic field, or by reversing the helicity of the photons when they are involved in the experiment, will give rise to dichroic effects that allow to access the spin arrangement, and the magnetic structure. In these cases, the information can generally not be extracted directly from the experimental data, especially when a high accuracy is needed. A comparison to a sophisticated theoretical model is necessary as well as computer modeling of the experiment, and it is only after a lengthy process of repetitive refinement of the model that the information can be extracted. But it is this procedure, although often tedious, that makes these spectroscopies so accurate (of the order of 0.001 nm for crystallographic determinations) and so popular. Indeed, a recent survey for a surface structure database[3] indicated that two-thirds of the solved surface structures had been produced by LEED while the rest was due essentially, in equal part, to XRD, PhD, XAS, and Ion Scattering (IS). This makes electron spectroscopies account roughly for five-sixths in the solving of surface structures. Moreover, for bulk properties, XAS is known as one of the leading techniques, and photoemission is unavoidable for bandstructure and Fermi surface mapping.[4]

The nanoscale, which deals with assemblies of several atoms, is intermediate between the mesoscale and the atomic scale. Hence, it will generally need a mix of qualitative and quantitative structural determination and therefore, electron spectroscopies are among the best suited tools available to study nanostructured materials as they are capable of giving both type of information.

We wish here to discuss in more detail the type of information they can provide and the best way to extract this information so that it is accurate enough to give a precise knowledge of the material under study. In the next section, we will discuss the most widely used techniques. We will classify them in Section 3 in relation to the expression of their cross-section and derive from it the type of information each of them can provide. Section 4 will be devoted to the methodology that is necessary to achieve a good accuracy. Then, two examples will be given in Section 5 to illustrate various points discussed in the previous section.

2 An overview of the different techniques

Electron spectroscopies are so numerous that we will not attempt to describe all of them here, even not try to list them. We will only discuss some of these techniques, generally the most popular ones, and classify them according to the type of information they can provide. We will relate this classification to the expression of their cross-section and see how differences in the expression of these cross-sections can explain the type of information they can provide. We just give here a brief outlook of the techniques we will focus on, and refer the reader to standard textbooks for a more detailed description, especially from the experimental point of view.[5-8]

2.1 LEED

LEED, and its various energy extensions such as MEED (Medium-Energy Electron Diffraction) or RHEED (Reflection High-Energy Electron Diffraction), is the oldest electron spectroscopy and the archetypal surface structure technique. There is an extensive literature on the subject to which we refer the reader.[9-11] Here, a beam of monoenergetic electrons is focused on the sample and the scattered electrons are collected by a detector or a hemispherical screen. Therefore, the wave function of each electron detected has gathered, through repeated scattering by the atoms of the sample, all the crystallographic information. Due to the low value of the electron mean free path in the energy range of a LEED experiment, typically 1 nm at most, this information is essentially related to the arrangement of the surface and subsurface atoms. But there is no chemical sensitivity, contrarily to most of the other electron spectroscopies, and therefore no localization of the scattering process around a particular atom. Hence, LEED is a long-range probe. Note that standard LEED requires a periodicity on the surface while diffuse LEED[12,13] (DLEED) does not and can give information around an adsorbate atom. The basic idea behind DLEED is very simple. The lack of translational symmetry prevents the formation of sharp spots in the LEED pattern, leading instead to a diffuse distribution of intensity. But at low temperature, adsorbed species tend to find the optimal adsorption site and stay there as their mobility is reduced. Then, all the adsorption clusters are structurally equivalent (this is called lattice gas disorder). Moreover, for a low coverage, it is most likely that no correlation will happen between different adsorption clusters. Hence, the total diffuse LEED pattern is equivalent to that of a single cluster, which gives access to the local structure.

Finally, spin-polarized LEED, with a spin detection, can be used to probe the magnetic structure.

2.2 XAS

The history of XAS coincides with that of synchrotron radiation as XAS was probably the first technique for the characterization of materials that was developed on synchrotron radiation beamlines. Contrarily to LEED, which is a laboratory-based technique, it requires a tunable source of photons and therefore it is almost always performed with synchrotron radiation, although laboratory sources do exist.[14] In a typical XAS experiment, a beam of monochromatic photons is directed onto the surface of a material. Then, the fraction of photons that escape this material is measured as a function of their energy. This gives a direct measure of the absorption properties of the material. As the photons are usually absorbed through the excitation of an electron on a given core level of a particular atomic species, the main features of the spectra are edges corresponding to the excitation of the various core levels. Above each edge, XAS probes the local structure around the corresponding atomic species.

Under the generic name of XAS, several spectroscopies have been developed for various purposes. XANES (X-ray Absorption Near Edge Structure) corresponds to the detection of absorption losses up to about 30eV above an edge. Due to the low kinetic energy of the electrons involved, these will essentially populate the empty states and therefore, XANES will give access to the density of these empty states. EXAFS (Extended X-ray Absorption Fine Structure) and SEXAFS (Surface EXAFS) involve electrons of higher kinetic energy and hence, they will probe the local crystallographic structure around the atoms where from the electrons originate, which will be mainly bulk atoms in the first case (photons penetrate deep into the matter) and surface ones in the second. There are many texbooks or review articles on the subject to which we refer the reader for a deeper understanding.[15-17] The discovery of sum rules[18] relating the signal measured in the dichroic mode to the magnetic structure has made XAS the leading electron-based technique for magnetic studies.

2.3 PhD

Photoelectron diffraction is a versatile technique that can be performed either with a standard laboratory XPS equipment or on a synchrotron radiation beamline. It is derived from photoemission : photons illuminate a sample and are absorbed through the excitation of electrons. The fraction of these electrons that can escape the sample are then analyzed for a given kinetic energy and escape direction. When monitored as a function of this energy or this direction, the signal measured exhibits strong modulations that can be related in an unambiguous way to the local structure around the atom that has

produced the corresponding electron. Hence, like XAS, it is chemically specific and localized (for core-level excitation), in contrast to LEED. Due to the low escape depth of the electrons, it is essentially a surface technique and can be used both in the spin-resolved and dichroic modes to access information on the magnetic structure. The extraction of the information from the modulations is slightly more involved than in XAS but the directional information such as the bond direction is here inherent to the technique and consequently can be obtained with a better accuracy than in XAS. For more details, we refer the reader to extensive review articles.[19-21]

2.4 AED

We will not discuss much Auger Electron Diffraction as it is very similar to PhD. It is nevertheless a very much used technique. It only differs from PhD by the way the electron that escapes the sample is produced. Here, this electron is excited through an Auger process which makes the interpretation of the AED modulations much more complicated unless one of the transition channels dominates the process.[22] There are so many Auger transitions that it is often possible to select the Auger process so that it is effectively the case. However, the neglect of second order transitions will certainly affect the accuracy of the structural determination.

2.5 EELS

Electron Energy Loss Spectroscopy is an extremely versatile laboratory-based technique. Its basic principle is close to that of LEED with the essential difference that the incident electron, multiply scattered by the atoms of the material, undergoes a loss on one of these atoms through the excitation of a second electron. This loss process introduces a localization which LEED lacks, but it introduces as well a higher degree of complexity in the analysis. Originally, EELS was designed to study collective excitations such as plasmons[23] or phonons, [24] and it is still one of the best tools for this purpose. Then, it was progressively realized through the use of the core-level excitation mode that it could be used as well to access information on empty states like in XANES, or for surface crystallographic characterization.[25-26] Indeed, in this mode, the cross-section of EELS is close to that of XAS[27,28] and hence, similar information can be obtained in principle from the analysis of its modulations. However, the complexity introduced by the presence of two electrons that can be both multiply scattered in their initial and final states makes the calculations rather long and tedious and has seriously limited the use of EELS for this kind of purpose up to now. Only a new step in the theoretical development can allow it to become as powerful and popular as LEED, XAS or PhD for surface structure determination and compete with them.

2.6 BIS

Bremsstrahlung Isochromat Spectroscopy is very similar to a time-reversed photoemission process in its principle except that it does not involve any core electron. This has important consequences on the interpretation of the spectra as the selection rules on the angular momentum eigenvalues will not be as simple as in the case of photoemission. In a BIS experiment, a beam of monoenergetic electrons is directed onto a sample. Within this sample, the electrons can decelerate and emit photons (this is termed the bremsstrahlung radiation). These photons are then monitored at a fixed energy, called the isochromat energy, as a function of the varying energy of the incident electron beam. Like in XAS or in angle-resolved photoemission, there are various energy ranges which differ on the type of information they can provide. When the energy of the decelerated electrons is small, BIS will give access to the total density of the unoccupied states, as the corresponding electrons will principally populate these states. For higher kinetic energies of the final state electrons, EXBIFS (Extended X-ray Bremmstrahlung Isochromat Fine Structure) will provide crystallographic information.

The main problem in BIS theory concerns the localization in space of the bremsstrahlung process. Šimunek and coworkers[29-31] showed that, because of the enormous electrostatic field needed for the deceleration to occur, it can only happen in the immediate vicinity of the atomic cores. Hence, the bremsstrahlung process is localized and furthermore, the dipole approximation is generally valid. Thanks to this, the cross-section of BIS is very similar to that of XAS provided that the multiple scattering of the incoming electron is not too important.

3 Classification of the techniques

There are several criteria that can be applied to

classify the electron spectroscopies depending on the property on which we want to make the distinction. The most obvious one corresponds to the alternative laboratory/synchrotron radiation center. Although it is often desirable to be able to make the experiment with a standard laboratory equipment (electron gun, photon source), this is not always possible in practice as the various electron spectroscopies do not give the same information and some of them need specifically a tunable source of photons of high flux and polarization to operate. For instance, if we take the techniques described in the previous section, LEED, EELS and BIS are exclusively laboratory-based techniques while XAS always needs a synchrotron radiation beam to give its best as no laboratory-based tunable source of photons can compete at present. PhD on the other hand can be performed in both cases but will generally lead to more accurate information with synchrotron radiation due to a good polarization of the photons and a better energy resolution thanks to the use of monochromatized photons (strictly speaking, photons emitted by a standard laboratory lamp can be monochromatized, but the flux is generally poor).

A second distinction that can be introduced concerns the initial state of the probe electron, *i. e.* of the electron that gathers the information we are seeking by repeated scattering by the atoms in the material. When the initial state is localized, in other words when the excitation process or the loss process takes place on a particular atom, the electron, due to its rather short mean free path, will probe essentially the structure (crystallographic, electronic or magnetic) around this atom. The information we will be able to extract from the signal monitored will therefore concern the short-range order in the immediate vicinity of the atom where the probe electron has been produced. On the contrary, when the initial state of this probe electron is rather delocalized, the corresponding technique will only be sensitive to long-range order and the information obtained will reflect the long-range structure of the sample. Localized spectroscopies include XAS, PhD/AED, EELS, when a core state in involved, as well as BIS and DLEED. Long-range probes comprise LEED, valence PhD, valence EELS.

There is at least a third criterion that can be used to distinguish the electron spectroscopies, which is whether the probe electron is effectively measured or not. In our view, it is the most important criterion as it will influence directly the form of the cross-section, *i. e.* the signal measured by the detector, and hence the type of information that can be extracted from it. Indeed, if the probe electron is measured and the initial state of this electron is well defined, then the detector selects only the electrons that were originally in this initial state and that have now the right energy. The cross-section for such an electron detected along the $\hat{k}$ direction can be simply expressed as[32]

$$\frac{\mathrm{d}\sigma}{\mathrm{d}\hat{k}} \propto \sum \left| < f \left| T \right| i > \right|^2 \qquad (1)$$

where $|i>$ is the initial state, $|f>$ the asymptotic final state of the electron (*i. e.* an eigenstate of H_o and not of $H = H_o + V$ where V is the potential of the whole system) and T is a transition operator characteristic of the selected electron spectroscopy. The sum runs over all relevant quantum numbers associated to $|i>$ and on the various atoms where the transition can take place. This type of expression includes LEED and PhD/AED. Now, when the probe electron is not detected, which is the case of XAS, EELS or BIS, or when the initial state is not known (for instance because it is scanned as in angle-resolved photoemission), the problem is totally different. Indeed, in this case the energy conservation of the corresponding electron through the transition process is not ensured anymore by the detector. As a consequence, it has to appear in the expression of the cross-section, together with a sum over all the electron states that satisfy this energy conservation. In this case, the cross-section becomes[32]

$$\sigma \quad \text{or} \quad \frac{\mathrm{d}\sigma}{\mathrm{d}\hat{k}} \propto \sum \mathrm{Im}\left[< K \left| V_t^{\dagger} G^{+} V_t \right| K > \right] \qquad (2)$$

Here, $|K>$ denotes the known state, either initial $|i^+>$ when the probe electron is not detected, or final $|f^->$ when the initial state is unknown. These states take into account all the multiple scattering processes undergone by the electron before it becomes the undetected probe electron ($|i^+>$) or after ($|f^->$). V_t is the potential responsible for the transition of this electron from its initial state to the probe state and is generally real. It can be a promotion or a loss mediated by a photon (case of XAS and BIS respectively where V_t is then the dipole operator), or by another electron (case of EELS where V_t is a Coulomb potential). In the latter case, all states and operators are

two-electron ones. G^+ is the propagator of the probe electron. Therefore, G^+ and $|K\rangle$ will not be evaluated at the same energy as V_t induces an energy change. As in the other case, the sum here runs over all relevant atoms and angular momentum quantum numbers of $|K\rangle$. Note that $\mathrm{Im}\left[\langle K|V_t^\dagger G^+ V_t|K\rangle\right]=\mathrm{Im}\left[\langle K|T_{DWBA}|K\rangle\right]$ where T_{DWBA} is the first order distorted wave Born approximation of the full system (*i. e.* with $V_{sample}+V_t$) transition operator.

It is clear from this discussion that whatever the case we are dealing with, the basic process remains the same. This process is simply the multiple scattering of the probe electron by the sample atoms, and the corresponding scattering of any other electron involved in the description of the technique considered, with a possible gain or loss of energy due to V_t. Therefore, all electron spectroscopies can be described within the same unifying framework.[33,34] A convenient way to construct this framework is to define the scattering path operator, which was originally introduced by Faddeev[35] to treat nuclear physics problems. In our case, this operator connects two atoms by describing all the pathways an electron can follow to go from the first atom to the second one. Hence, it takes into account all the multiple scattering that affects this electron on its way from one atom to the other, including the scattering by these two atoms. For a process describing an electron originally scattered by atom i and that eventually ends by being scattered by atom j, it is generally noted τ_{ji}. Its expression as a function of the potentials V_i and V_j of the two extremity atoms (in between, the electron is scattered by all the atoms of the sample) is simple to derive[34]

$$\tau_{ji} = V_j \delta_{ji} + V_j G V_i \tag{3}$$

Here, G is the propagator of the full system. The physical meaning of this expression is then straightforward. In terms of the transition operators of the individual atoms, which are the quantities that are meaningful for us when working with eigenstates of the unperturbed Hamiltonian (these states are the only known states prior to any calculation), the scattering path operator follows the equations of motion[34]

$$\begin{cases} \tau_{ji} = T_j \delta_{ji} + \sum_{k \neq j} T_j G_o \tau_{ki} \\ \tau_{ji} = T_j \delta_{ji} + \sum_{k \neq i} \tau_{jk} G_o T_i \end{cases} \tag{4}$$

Now, G_o is the free electron propagator, *i. e.* the propagator corresponding to the unperturbed Hamiltonian H_o. Note as well that due to the generalized Faulkner-Stocks decomposition,[34,36] the propagator G is proportional to any matrix element of the scattering path operator τ.

It is not our purpose here to give a full account of the derivation of the cross-section of the major electron spectroscopies within a scattering path operator description. This can be found elsewhere[32]. But one of our aims is to demonstrate how the expression of these cross-sections can explain the type of information that we will be able to extract from the signal of the corresponding spectroscopy, the similarities and differences between these spectroscopies and how they can be enhanced or diminished by playing with the energies of the beams involved, or with the geometry.

The cross-sections of the electron spectroscopies we have considered so far in this review can be related to particular values of the scattering path operator[32]. If we note 0 the atom on which the physical process responsible for the localization, if any, takes place, then these cross-sections are function of the following elements of

$$\tau \begin{cases} \tau_{ji} & : \text{LEED, valence PhD, valence EELS} \\ \tau_{j0} & : \text{core PhD/AED} \\ \tau_{00} & : \text{XAS} \\ \tau_{00} \text{ and } \tau_{0i} & : \text{BIS} \\ \tau_{00}, \tau_{0i} \text{ and } \tau_{j0} & : \text{core EELS} \end{cases} \tag{5}$$

for all atoms i and j in the sample. The distinction between localized and non localized spectroscopies is clear here as the latter involve τ_{ji} with j and i scanning all the atoms in the sample. Therefore, no short-range information can be extracted from the signal as no particular atom is singled out. In contrast, localized spectroscopies involve either τ_{00}, τ_{j0} or both (τ_{0i} can be obtained from τ_{i0} by a reversal of the direction of propagation) and hence, the local structure around atom 0 is contained in these matrix elements of the scattering path operator. In the case of τ_{j0}, an explicit escape direction is present in the element and it will therefore be much more sensitive to angular parameters than τ_{00}.

Let us focus now in more details on the localized electron spectroscopies. We see clearly from (5) that two techniques, XAS and core PhD/AED can be considered

as the basic ones as far as the type of information they contain is concerned. With this in mind, core EELS and BIS for instance can be understood as a combination of these two basic spectroscopies according to a complex pattern. This means that both type of information, that more radial of XAS present in τ_{00} and that intrinsically directional of PhD/AED contained in τ_{j0} can in principle be extracted from the same experiment provided that the corresponding scattering path operators are sensitive enough to the parameters of interest. They always coexist, but the way they mix together makes the extraction of the information much more complex than in the case of XAS or PhD/AED. Nevertheless, as in these spectroscopies τ_{00}, τ_{j0} and/or τ_{0i} are evaluated at different energies corresponding respectively to that of the probe electron, the outgoing and/or the incident electron, it is possible to play with these energies to simplify the analysis of the data. Indeed, due to the strong forward peaking of the scattering factor at medium and high energies, it is possible to minimize or maximize multiple scattering effects in the directional τ_{j0} and τ_{0i} scattering path operators so that either them or τ_{00} are reinforced to dominate the total signal. Note that most EELS and BIS codes totally neglect the multiple scattering effects in the incoming and/or outgoing electron beam as they are based on XAS codes. Provided that an accurate and fast code exists to simulate EELS and BIS (which is not yet the case), we see as well that they can in principle give both the electronic and crystallographic structure information in the same experiment as the access to one or the other is simply a matter of energy range.

This discussion makes it clear that sophisticated calculations are necessary to extract an accurate structure information from the experimental spectra. We will see now what are the best ways to do it.

4 Methodology

Obviously, the ideal and simplest strategy would be to be able to extract the information directly from the experimental spectra, without having to resort to a complex theoretical analysis. This is called the direct or inverse method. Such methods exist for the various spectroscopies, and we will discuss them later. However, as the particles involved are mainly electrons whose propagation is extremely anisotropic, all of them rely on severe approximations and therefore, if their accuracy is sufficient in the mesoscopic scale, they certainly cannot be used on their own on an atomic scale. This means that if we need the latter sort of accuracy for solving a structure, there is no other way than to calculate the spectra using a theoretical model and compare the result to the experiment. This is the error and trial method. As we have seen in the previous section that the structure information we are looking for is contained in the matrix elements of τ, it is clear that most of the theoretical work will concern the computation of τ, or of related quantities (non localized techniques such as LEED being long-range probes, they rather use a plane partitioning approach so that space-group symmetries can be incorporated easily to decrease the amount of computing to be done). This includes all the multiple scattering description and can be therefore long and tedious depending on the number and type of matrix elements of τ that need be computed (τ_{00} will be fast to calculate while τ_{j0} will take a lot of time if the contribution of each terminal atom has to be computed separately). Of course, each such calculation has to assume a structure (crystallographic, but although electronic and magnetic if necessary) so that τ can be evaluated. There is no reason for this assumed structure to be the real one as the latter is supposed to be unknown. Therefore, we see clearly here that the whole process will have to be repeated for several trial structures before a calculation coincides, within the experimental error, with the experimental data. Hence, although most accurate, the error and trial method can take an enormous amount of computing time before a structure is solved with, in addition, the possibility for the real structure never to be found if it differs sensibly from all the structures that have been tested. Consequently, a strict methodology is necessary both to reduce the amount of calculation time and to increase the probability of effectively solving the structure problem. This methodology can be decomposed into four steps which we will now discuss successively: 1) choosing an approximate trial structure; 2) simulating the corresponding cross-section; 3) comparing to the experimental data; and 4) exploring the parameter space to produce a new trial structure. These steps are represented as a flowchart in Fig.2.

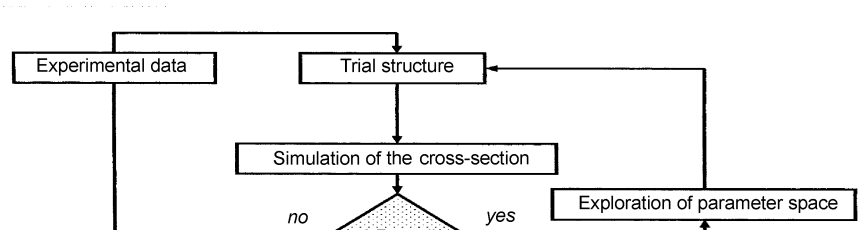

Fig.2 The flowchart corresponding to the four step methodology used to solve a structure. Here, ΔR represents any variation in the structural parameters.

4.1 Choosing an approximate trial structure

This is of course a key step in the whole process. The closer this approximate structure from the real one, the less computational effort. Basically, there are just two possibilities. The favourable one is that some information is already available in the literature, that was determined by some other technique. In this case, it is essentially a matter of refining the structure and the logical starting point is the structure as it is already known. Alternatively, if it is the first time this material is studied and no information is available or can be deduced from similar materials, the problem is more acute. Then, the only way to find a reasonable approximate structure as a starting point for the simulations is to use one of the direct methods we mentioned previously to solve the structure, or part of it, on a lower length scale. We will here review briefly four of them : the Fourier transform, the projection method, the holographic transform and circular dichroism in angular dependence (CDAD).

4.1.1 The Fourier transform method

It is the oldest inverse method[37] and can be applied to any localized spectroscopy in a backscattering geometry. It has been used extensively in EXAFS for several decades and has been adapted more recently to PhD.[38,39] Obviously, it can only be used when the modulations in the experimental data are obtained from an energy monitoring $I(\vec{k})$ of the individual spectra. When these modulations are dominated by those caused by a particular process such as single scattering backscattering by the nearest neighbours, the Fourier transform will give an immediate access to the pathlength of the corresponding process. These modulations are normalized to obtain the modulation function where I_0 is an average of the data that represents the purely atomic (*i.e.* unscattered) contribution. The Fourier transform $F(\hat{k},r)$ (if there is an escape direction $\hat{k}$ for the electron; otherwise, it is only a function of r) is obtained as

$$F(\hat{k},r)=\int_{-\infty}^{+\infty}\chi(\vec{k})e^{-ikp(\vec{r})}dk \tag{6}$$

The function $p(\vec{r})$ represents the pathlength difference between the unscattered and the scattered beam of electrons when they travel from atom 0 where they are produced to where they take their final state. Therefore, the Fourier transform can be seen as a projection of the energy modulations $\chi(\vec{k})$ onto the pathlength difference phase factor. To be of any practical use, the pathlength

difference $p(\vec{r})$ must be a simple function of the position of the atoms. Hence, the only practical solution is to restrict it to its single scattering expression, *i. e.* $p(\vec{r}) = kr - \vec{k}.\vec{r}$, where $\vec{k}$ is the final state wave vector of the electron. For EXAFS or PhD in a backscattering geometry (for instance from an adsorbate core level), this single scattering pathlength difference becomes $p(\vec{r}) = 2kr$ as only the τ_{00} terms, *i. e.* paths starting and ending on atom 0 contribute or are significant, while for PhD in general it is $p(\vec{r}) = kr(1-\cos\vartheta)$ if ϑ is the angle between the bond direction $\vec{r}$ and the escape direction $\hat{k}$. By construction, the Fourier transform (6) will exhibit maxima for values of r corresponding to neighboring atoms in the sample and for escape directions, if any, coinciding with bond directions.[39] Note however that for forward scattering processes in PhD, there is no pathlength difference and hence these processes do not contribute to the Fourier transform, even if they dominate the signal $\chi(\vec{k})$. From this discussion, it is clear that the accuracy of such a crystallographic determination will be limited by at least three factors: the neglect of multiple scattering, that of the scattering factor that sensibly alters the shape of the electron wave function (the Fourier transform was adapted from X-ray techniques where the propagation of the light is isotropic), and the averaging on inequivalent sites. Indeed, when electrons can be produced on atoms having a different geometrical environment, the Fourier transform method will give an average of the local geometric structure around these different atoms as it cannot discriminate between them. This can be readily seen in Fig.3 where a contour map of $F(\hat{k},r=0.4\text{nm})$ for PhD is shown for the adsorption system Cu(111)-C_2H_2.[40] Here, there is an apparent sixfold symmetry because of the superposition of the nearest-neighbors positions of the two unequivalent carbon absorbers shown in the inset, which can mislead the interpretation. A correction for the scattering factor can be applied using tabulated values of this scattering factor. This is currently done in EXAFS, but it is far from satisfactory. However, this particular problem can be remedied for quite easily, *albeit* to the price of a sensible increase in the complexity of the method. This leads to the projection method.

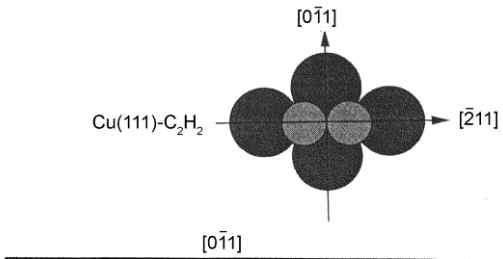

Fig.3 360° contour map of the square of the Fourier transform amplitude at $r = 0.4$ nm from PhD spectra taken in the [1$\bar{2}$1], [2$\bar{1}$1] and [$\bar{1}$10] azimuths for the adsorption system Cu(111) -C_2H_2.[40]

4.1.2 The projection method

This inverse method was proposed by Hofmann and coworkers[41] as a direct improvement of the Fourier transform method for PhD in a backscattering geometry. It can be adapted, of course, to any other localized electron spectroscopy in the same geometry. The basic idea is to cure the previous method from the lack of a proper scattering description, *i. e.* to introduce the effect of the scattering factor. Hence, the change is quite straightforward: the projection is made now on the single scattering modulation function $\chi_{th}(\vec{k},\vec{r})$ for a single scatterer which contains both the pathlength difference phase factor and the scattering factor. Now, the projection coefficient $c(\vec{r})$ is given by

$$c(\vec{r}) = \int \chi(\vec{k})\chi_{th}(\vec{k},\vec{r})\,\mathrm{d}k \tag{7}$$

However, $\chi_{th}(\vec{k},\vec{r})$ contains an attenuation term (1/*r*) and therefore diverges on atom 0 . To by-pass this problem, we take an exponential and form the function[42]

$$C(\vec{r}) = \sum_i \mathrm{e}^{c_i(\vec{r})r} \tag{8}$$

Here, several experimental modulation functions for different emission directions are combined (hence the summation over i) to improve the accuracy. $C(\vec{r})$ gives some measure of the probability of finding a substrate atom at the position $\vec{r}$ on the grid used to calculate $\chi_{th}(\vec{k},\vec{r})$. Therefore, strong maxima should appear at the location of the nearest neighbors. Such an example is given in Fig.4 for the PhD from the system Cu(111)-OCH_3 whose geometry is sketched in the inset. The crosses indicate the position of the Cu atoms as obtained from a multiple scattering calculation when an O 1s core level is excited, and the elongated parabolae correspond to the largest values of $C(\vec{r})$.[41]

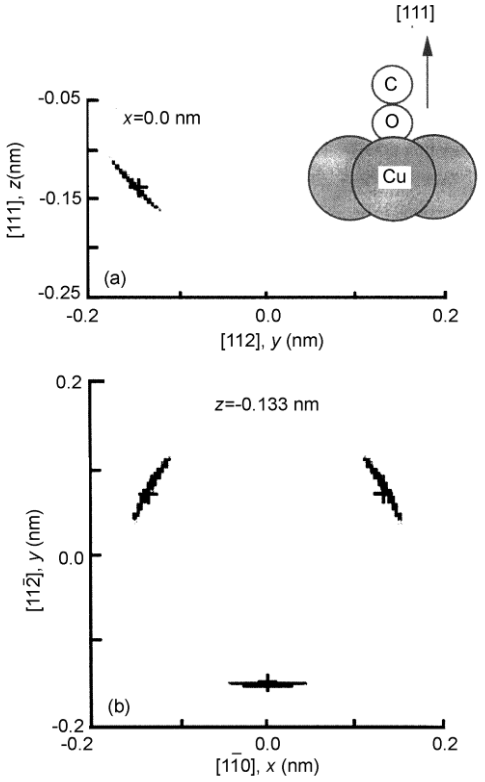

Fig.4 The coefficient $C(\vec{r})$ for the system Cu(111)-OCH_3. (a) corresponds to the *xy* plane at *x* = 0.0nm and (b) to the *xy* plane 0.133nm below the emitter. The inset shows the resulting structural model (the H atoms are not shown). The crosses indicate the positions of the atoms derived from multiple scattering calculations.[41]

4.1.3 The holographic method

The holographic method is closely related to the two previous ones, although it was developped in a very different context. It was proposed originally, for electron spectroscopies, by Szöke[43] as a way to reconstruct, from the experimental data, a 3D image of the surface of the sample. The ultimate goal was to eventually obtain the crystallographic information directly from the data, without comparing to a calculation but with the same accuracy. It is now realized that such an aim is unachievable due to the many limitations arising from the fact that the propagation of the electrons is not isotropic, in contrast to the optical case. Anisotropies due to the directionality of the initial state wave function, to that of the scattering process, will add to the multiple scattering to damage the accuracy unless seriously reduced by corrections that are often case-dependent as to their efficiency. Therefore, it cannot be considered now as more than an inverse method that will give an approximate structure of the sample.

Up to now, holographic methods have been developed for PhD,[44] for both standard[45] and diffuse[46] LEED and XAS.[47] We will only focus, in this discussion, on the PhD case which is both historically the first one and the simpler.

A hologram simply consists in the modulation function $\chi(\vec{k})$ mentioned previously. It contains all the interference information that will allow the reconstruction of the image as in the optical case. The first problem with this hologram is that it contains in fact more than this and the extra information will distort the reconstructed image. Indeed, if we decompose the signal measured into

$$I(\vec{k}) = \left|\psi_r + \psi_o\right|^2 \tag{9}$$

where ψ_r is the reference wave, *i. e.* the unscattered one, and ψ_o the object (scattered) one, then

$$\chi(\vec{k}) = \frac{\psi_o}{\psi_r} + \frac{\psi_o{}^*}{\psi_r{}^*} + \frac{\psi_o\psi_o{}^*}{\psi_r\psi_r{}^*} \tag{10}$$

The first term is the holographic term itself, the second is the twin term and the last one the self-interference term. In the reconstruction process, the holographic term will give the image while both extra terms will lead to artifacts.

Originally, the holographic method was developed into two directions, for energy scans and for angular ones. Now, it is recognized that the only way to minimize the

effect of the twin and self-interference term on the one hand, and of the multiple scattering on the other hand, is to perform the holographic inversion either from an energy scan for several directions of detection, or from an angular scan for several energies, which leads to the same result as in both cases, many angles and many energies are needed. Actually, it is now clear[48] that the best images are achieved with 5 to 10 energies and a 5 to 10 degree spacing for the angles, which amounts to about 6400 spectra to be recorded. Clearly, the holographic method needs an enormous experimental investment.

The PhD holographic reconstruction is obtained by

$$U(\vec{r}) = \int \chi(\vec{k}) K(\vec{k}, \vec{r})\, \mathrm{d}\vec{k} \tag{11}$$

where now multiple energy and angular points are taken. $K(\vec{k}, \vec{r})$ is the reconstruction kernel function. In the SWIFT (Scattered-Wave Included Fourier Transform) algorithm,[49] it is given by

$$K(\vec{k}, \vec{r}) = \frac{\mathrm{e}^{i(\vec{k}.\vec{r}-kr)}}{M(\hat{\varepsilon}, \vec{k}) f(\vartheta)} \tag{12}$$

It corrects the standard Fourier transform for anisotropies generated by the initial state (hence the optical matrix $M(\hat{\varepsilon}, \vec{k})$ describing the optical transition undergone by the electron) and by the scattering factor $f(\vartheta)$.

In the SWEEP (Small-Window Energy Extension Process)[50,51] case, it becomes

$$K(\vec{k}, \vec{r}) = \mathrm{e}^{i(\vec{k}.\vec{r}-kr)} W(\hat{k}.\hat{r}) \tag{13}$$

Now, $W(\hat{k}.\hat{r})$ is a window function that limitates the anisotropies by restricting the reconstruction process around the backscattering or the forward scattering directions.

Apart from the twin and the self-interference terms we have already mentioned, the hologram $\chi(\vec{k})$ is prone to another endemic problem. Due to the strong forward peaking of the scattering factor at medium and high energies, where the ideal resolution $\delta r \approx 2\pi / k$ is the most favourable, holograms are dominated by very bright spots corre sponding to these scattering events. Now, as forward scattering corresponds to a no path-length difference, these spots do not contain any holographic information, and therefore prevent from really imaging forward scattering atoms as the interference fringes around containing the holographic information are generally not visible due to the extreme brightness of these spots. Two promising techniques have been devised to solve this problem. The first one is called near-node holography.[52] It consists in decreasing the brightness of the forward scattering peaks and increasing that of the fringes by choosing the experimental geometry so that the forward scattering direction is near a node of the wave function of the emitted electron. Hence, the forward scattering peaks are more or less suppressed from the hologram while the interference fringes are then clearly visible. The holographic reconstruction can then image up to the second nearest neighbours. This can be seen from Fig.5 where both standard and near node holograms (5a and 5c) and holographic reconstructions (5d and 5f) are presented.[52] In the standard case, the hologram is dominated by the bright forward scattering spots whose positions can be derived directly from the stereographic projection (5b) of the high density chains and planes. On the contrary, the interference fringes are clearly visible in the near node geometry hologram and they allow a much better imaging of the Al(111) surface atoms sketched in 5e.

The second technique is differential holography.[53] It is based on the fact that the interference fringes vary much more quickly with k than the forward scattering peaks. Therefore, the substraction of two holograms for close k will remove most of the peaks without suppressing too much of the fringes.

4.1.4 Circular dichroism in angular dependence

This method has been established recently[54] for PhD. It originates from the fact that forward scattering peaks are shifted in azimuth when the helicity of the photons is reversed. This peak rotation can be described by the approximate formula[54]

$$\Delta\varphi \approx \frac{m^*(\vartheta)}{kR\sin^2\vartheta} \tag{14}$$

where R is the emitter-scatterer distance, ϑ the scattering direction and $m^*(\vartheta)$ is an effective azimuthal quantum number depending upon the scattering direction, but that can be calculated easily.[54]

For a neighbor direction (ϑ, φ), the forward scattering peak will appear at $(\vartheta, \varphi \pm \Delta\varphi)$ when reversing the helicity of the photons. Consequently, the direction of

the scatterer is the mid-point between the two directions observed experimentally. Then, the distance to the emitter can be obtained from (14) as

$$r = \frac{m^*(\vartheta)}{k\Delta\varphi \sin^2 \vartheta} \tag{15}$$

It should be noted that this method is very simple compared to the holographic one, and that it makes use only of the non holographic forward scattering peaks.

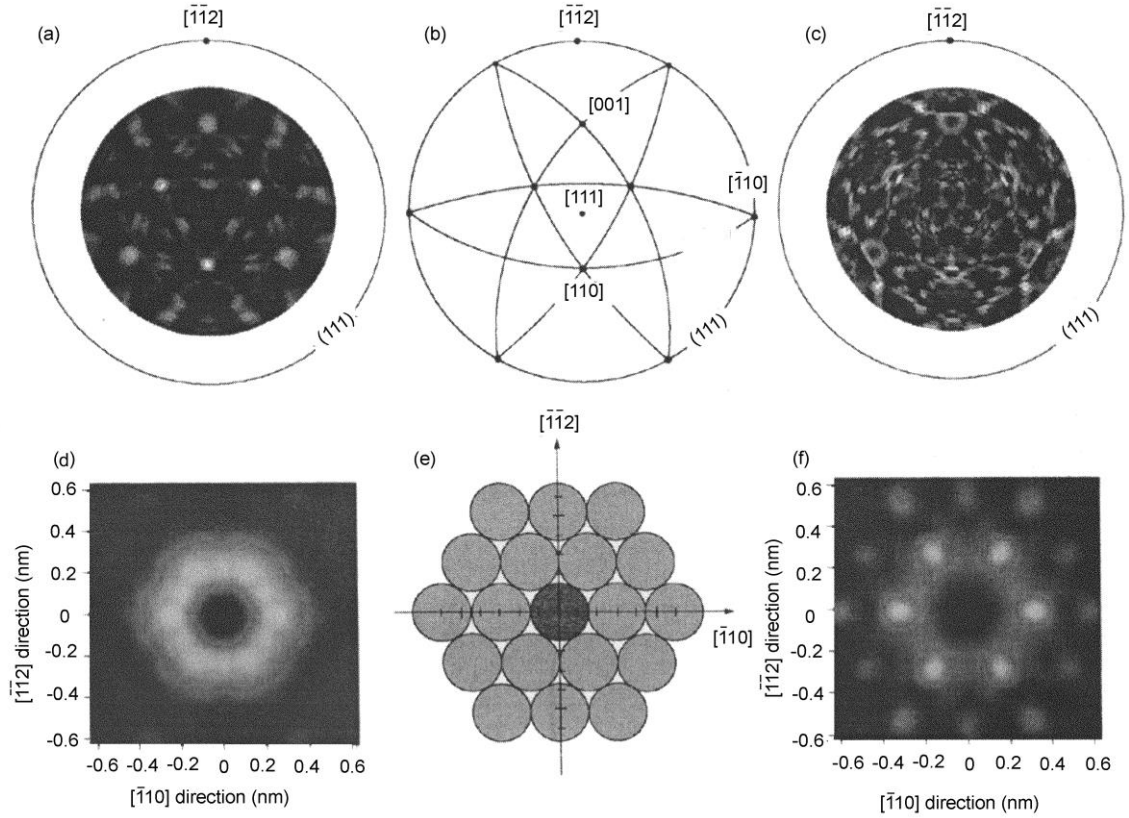

Fig.5 Comparison of far node and near node PhD data and their holographic reconstructions. (a) and (c) : stereographically projected experimental Al 2s (E_{kin} = 952 eV) PhD patterns from an Al(111) single crystal. In the far node geometry (a), forward scattering dominates the pattern as can be seen from the stereographic projection of the high density crystal chains and planes (b). In the near node hologram (c), no distinct forward scattering features are visible. (d) and (f) : corresponding holographic reconstructions of a plane parallel to the surface that contains the emitter at (0,0). They should show the expected image of an Al(111) plane (e). In the near node reconstruction (f), nearest, next nearest and second nearest neighbors are clearly resolved as local maxima while in the far node picture (d) no clear atom position can be seen.[52]

4.1.5 Accuracy of the direct methods

There is no real difference in the respective accuracies obtained by the different inverse methods presented in the previous paragraphs. Although many parameters can affect these methods, they cannot give distances within more than 0.02 nm at best. In the case of holography, the spatial resolution is given by[55]

$$\begin{cases} \Delta x = \Delta y &= \dfrac{2\pi}{2k\sin\vartheta} \\ \Delta z &= \dfrac{2\pi}{k(1-\cos\vartheta)} \end{cases} \tag{16}$$

This shows that the images will be elongated along the z direction.

For the CDAD, it is given by[54]

$$\Delta r = \frac{r^2 k \sin^2 \vartheta}{m^*(\vartheta)} \Delta\varphi$$

(17)

There, the accuracy on φ can be estimated to 0.3 to 0.5 degrees.

4.2 Simulating the cross-section

This is the longest part of the whole process by far. Indeed, here the whole multiple scattering problem has to be treated as accurately as possible to be able to extract the best information from the experimental data. We can face two cases here: either the structure for which the cross-section must be calculated is new, or very different from the previous one (let us recall that in the methodology we have defined earlier, many structures have to be tested against the experiment), or it is just slightly different from the one that has just been computed. In the former case, a full calculation has to be performed, while in the latter, a first order treatment, such as the one obtained by linearizing the multiple scattering equations, is sufficient, at least to indicate whether the modifications to the structure go into the right direction or not.

4.2.1 Full calculation

Many theories have been constructed to calculate the cross-section of electron spectroscopies, but basically they can be divided into two groups: cluster methods and slab ones. In the first case, the material is reduced to a small size cluster, taking into account the small value of the mean free path of the electron. Then, the wave function of the electron is expanded into spherical waves around each atomic center in the cluster. Historically, this was how the theory of localized spectroscopies such as XAS,[56,57] PhD,[58,59] EELS[27]or BIS[29-31] was derived. The other approach involves a partitioning of the material into planes so that the periodicity of each plane can be taken into account. As a consequence, the wave function of an electron incident upon such a plane is expanded into a set of discrete plane waves satisfying the cyclic conditions of that plane, while within a plane, it is expanded into spherical waves centered on the atoms of the plane. This approach is particularly suited to spectroscopies reflecting the long-range order and it is generally known as the standard LEED theory.[9-11]

Although these two methods seem very different at first sight, they can be shown in fact to be two particular cases of a more general theory based on multiple scattering in a partitioned space.[60]

4.2.2 Linear methods

The invention of tensor LEED[61] in the mid-eighties was a major breakthrough for the development of electron spectroscopies as, thanks to the enormous gain in CPU time, it opened the way to a systematic solving of crystal structures such as the one we have outlined in our four step methodology. Then linear methods were developed for LEED and other spectroscopies.[62,63] The basic idea behind these approximate methods is that when structural parameters in the material are changed by a very small amount, a first order perturbative approach should be sufficient to evaluate the changes induced in the cross-section. In other words, if $\psi(\vec{R}_1,\vec{R}_2,...,\vec{R}_N)$ is the wave function of the electron in a reference structure containing N atoms located at $\vec{R}_1,\vec{R}_2,...,\vec{R}_N$, then one has to the first order in $\Delta\vec{R}_j$

$$\psi(\vec{R}_1+\Delta\vec{R}_1,\vec{R}_2+\Delta\vec{R}_2,...,\vec{R}_N+\Delta\vec{R}_N)=\psi(\vec{R}_1,\vec{R}_2,...,\vec{R}_N)+\sum_{i=1}^{N}\Delta_i\psi \tag{18}$$

where $\Delta_i\psi$ is the correction due to the displacement of atom i alone :

$$\Delta_i\psi=\psi(\vec{R}_1,...,\vec{R}_i+\Delta\vec{R}_i,...,\vec{R}_N)-\psi(\vec{R}_1,\vec{R}_2,...,\vec{R}_N) \tag{19}$$

Note that (18) being a first order perturbation expansion is exact within the single scattering limit. Hence, in the linear method, the approximations will only affect the multiple scattering terms. The basic ingredients here are the wave functions corresponding to the displacement of any atom i alone, *i.e.* $\psi(\vec{R}_1,...,\vec{R}_i+\Delta\vec{R}_i,...,\vec{R}_N)$. They can be then either approximated themselves by a first order expansion, thus giving the tensor method (which is exact in the limit where a single atom is displaced), or calculated exactly by one of the methods of the previous paragraph, which is more time-consuming but much more accurate. This is the linear method as such.

The gain in the number of operations to be performed can be estimated quite easily.[64] For m scatterers that can take n positions each, the conventional method will need n^m full multiple scattering calculations to explore all the possibilities, while the linear ap-

proach based on Eq.(18) will only necessitate to compute nm full multiple scattering calculations, from which the n^m linear combinations can be obtained in a comparatively negligible time.

The validity of these methods can be estimated to 0.01 to 0.02 nm for the tensor one, and 0.02 to 0.05 nm for the linear one. But this domain of validity is an average and movements that make or break an alignment between atoms will not be well approximated by this approach as they make or break strong multiple scattering pathways. This is clear from Fig.6 which shows PhD simulations[64] performed with a full multiple scattering approach and with a linear one in the case of a three atom chain with the emitter at the bottom. When the two scatterers are moved off-axis (*i. e.* perpendicularly to the chain) in opposite directions by the same distance *d*, the linear approximation breaks down very quickly as can be seen both from the *R*-factor and from the comparison between the two curves.

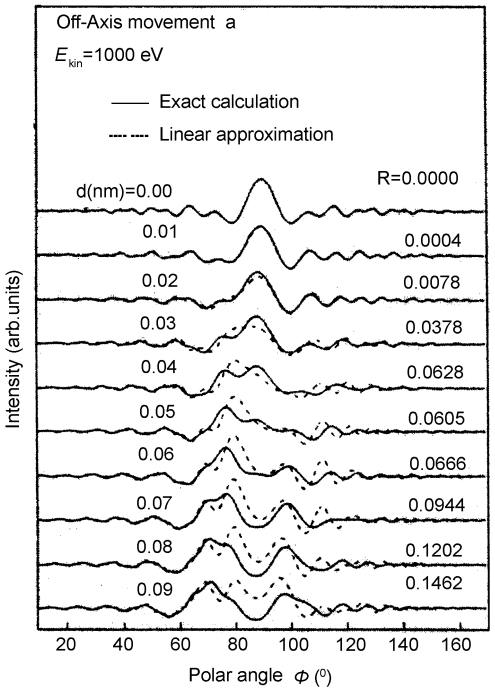

Fig.6 PhD curves obtained for a kinetic energy of 1000 eV with an exact calculation and the linear approximation for off-axis movement of the two scatterers of a three atom chain. The distance between the atoms is set to 0.256 nm when they are aligned. Then, the two scatterers are moved off-axis by *d* in opposite directions.[64]

4.3 Comparing to the experimental data

If a comparison by eye between a simulation and the experimental data is often necessary, it is neither accurate nor possible in the course of an automated structure search such as our four step one. The problem of the numerical comparison between two data sets has been adressed in the early days of LEED by several people. They came up with various definitions of reliability factors, usually called *R*-factors, in the manner of what was done in X-ray crystallography. The major issue when choosing a *R*-factor is to decide what features of the curves are the most important in a comparison, as a given *R*-factor will not be sensitive to all of them. Such features can be the peak positions, the relative peak heights or their widths for instance. A detailed and critical analysis of the various *R*-factors used in LEED can be found in the book by Van Hove, Weinberg and Chan[11]. We give here as an illustration a few examples of *R*-factors. The two most standard and simple ones are given by

$$\begin{cases} R_1 = \dfrac{\sum_n \left| I_{\exp}(n) - I_{th}(n) \right|}{\sum_n \left| I_{\exp}(n) \right|} \\ R_2 = \dfrac{\sum_n \left[I_{\exp}(n) - I_{th}(n) \right]^2}{\sum_n I_{\exp}(n)^2} \end{cases} \qquad (20)$$

Here n is the index of the point in the data set. These two *R*-factors are essentially sensitive to the relative peak heights.

Two corresponding *R*-factors R_1' and R_2' can be worked out by comparing the derivatives of the intensities, $I_{\exp}'(n)$ and $I_{th}'(n)$, instead of the intensities themselves as in (20). The main effect now will be to remove from the comparison most of the background that would not have been filtered out before. Other *R*-factors make use of the second derivatives, or of a combination of the first and second derivatives.[65] As they have been built to put the emphasis on different features in the comparison, there is no reason for the various *R*-factors to have the same behaviour when varying the structural parameters, although they often do. Therefore, in certain cases, it might be more profitable to use a combination of the results given by different *R*-factors to orientate the automated search.[66] Such an example is given in Fig.7 where different *R*-factors are shown for the PhD from W(110). These *R*-factors are plotted as a function of the dilatation or contraction of the first interlayer distance. *R*-factor 1 and *R*-factor 2 are equivalent to the R_1 and R_2 defined in Eq.(20) while

R_1' and R_2' correspond to *R*-factor 4 and *R*-factor 5 respectively. We clearly see here that all these *R*-factors oscillate strongly as a function of the interlayer spacing, and that the global minimum depends on the definition assumed. These oscillations in the parameter space are the main problem connected with *R*-factors. Indeed, this means that one has to be very cautious in a structural search. If the number of structures tested is not large enough to explore most of the parameter space, we can mistake a local minimum for the global one. Likewise, if the grid of an automated search is too coarse, there is a risk of being trapped in a local minimum. On the contrary, if this grid is too small, a lot of unecessary calculations will be made. Therefore, a good strategy is to find a systematic but thoughtful way to explore the parameter space and delimit more precisely the region where the real structure lies.

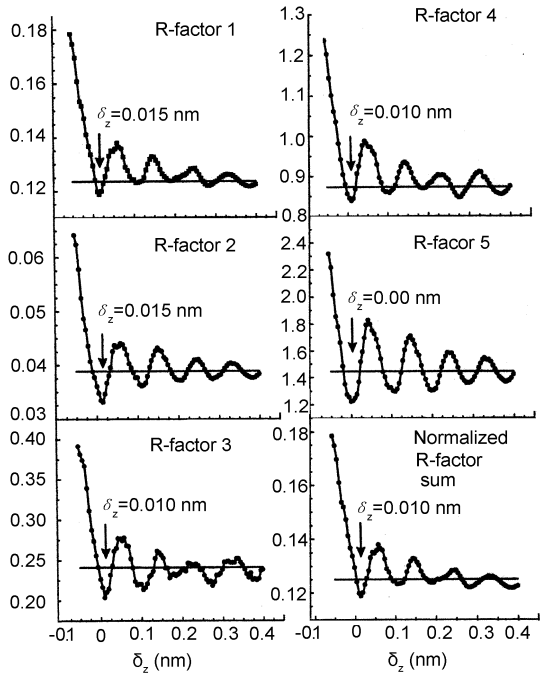

Fig.7 *R*-factor comparison of experiment and theory as a function of the interlayer relaxation δz relative to the bulk separation in W(110).

4.4 Exploring the parameter space

The simplest way to explore the parameter space is to use an equally spaced grid. But, as we have just discussed it, it can lead to a wrong structure if this spacing is too large or to too many calculations in the opposite case. Moreover, most of the parameter space is of no real use but it is not generally known *a priori* on which region to focus the search. Hence, a cleverer approach would be to find a strategy that is able to get out quickly of an uninteresting region and that will not be trapped in a false solution. We will review here the most frequent optimization methods used in the literature and the more promising ones.

4.4.1 Standard optimization methods

These are the most basic methods and they can generally only do local optimization, which means that they rely on local steps from the current solution, starting from the approximate structure used as the first trial structure. Then, they adapt the new candidate solution for the structure in the direction of the largest error decrease. For this reason, they are often called steepest-descent search algorithms. The direction in which they adapt the structure can be determined either by calculating the derivative of the actual position (gradient methods) or by making trial steps (simplex method). Then the search is finished when no more improvement can be obtained. Therefore, these methods will find the minimum which is the closest from the starting structure. In complex cases, this minimum has every chance to be a local minimum, leading then to a wrong solution.

4.4.2 Simulated annealing

Simulated annealing is part of what are called the global optimization methods, although strictly speaking it is not completely global. It mimics the process which makes a liquid crystallize when cooled gradually: the atoms loose mobility and then often form a pure crystal completely ordered which corresponds to a global minimum energy state. This is in contrast to rapid cooling where the liquid falls into a polycrystalline or amorphous state, corresponding to a local minimum with higher energy than the pure crystal state. The local optimization methods we have reviewed so far have the same behaviour as this rapid cooling process. In simulated annealing on the contrary, occasional jumps outside the barriers limitating the local minimum are allowed. In practice, it means that if the result of the *R*-factor is smaller than what was found for the previous structure, the new structure is kept and the self-consistent search cycle can start again. If it is larger, the new structure has still a

probability to be kept. Therefore, the simulated annealing algorithm can in principle find the global minimum, although there is no total guarantee as the jumps in the parameter space are made at random, and the computing time is usually limited. But the only real weakness of the existing algorithms is that they do not keep the memory of the past attempts, and they do not learn from these because of the randomness of the jumps. This means that they can explore several times the same local minimum and forget a deeper one.

4.4.3 The genetic algorithm

This approach has been devised to correct for the weaknesses of the previous one. The most important difference with the other search algorithms we have reviewed so far is that the genetic algorithm does not work with one structure that is then amended, but it makes use of a population of several trial structures. Its essence is to mimic the evolution of species using the same intrinsic laws that govern it. Each structure, *i. e.* each set of its M atoms, is encoded into a binary string which is called a chromosome. At the beginning of the search, a population of N chromosomes is created from a random exploration of the parameter space. A fitness value based on its R-factor is associated to each structure. Then, at each step of the search process, a new generation of population is produced from the previous trial structures by hybridization (also called mating or cross-over), mutation or selection while still ensuring the diversity of the species. The hybridization operation consists in cutting two parent chromosomes at a random position, or with a selective purpose in mind. Two children are formed by the recombination of the opposite fragments. A mutation is obtained by a change in the binary bits of a chromosome. Again, this can be done at random or through the analysis of previous mutations. Then, once N children have been created in these ways, both populations, the parents and the children, are compared and members of the parent generation can be allowed to replace chromosomes of the children one if their fitness value is higher. This is called survival of the fittest and it ends the process of the creation of a new generation.

This approach has many advantages over the other schemes. In particular, the deepest minimum encountered at a given stage of the process will not be forgotten because it has a high fitness value. Similarly, comparably good local minima will usually be remembered. The cross-over process will tend to keep the good aspects of the old structures and recombine them to try to produce better ones. It should be noted that the fact that the diversity of the population is always required means that when a member of the population gets trapped in a local minimum, the other members will tend to avoid this region of the parameter space. Note as well that the whole algorithm is independent of the problem; only the fitness function, a *R*-factor in our case, can be problem-dependent.

Preliminary tests conducted for LEED seem to indicate that the genetic algorithm is more efficient than simulated annealing.[67] Moreover, it contains many internal parameters that can be adjusted to increase its efficiency. Indeed, as discussed by De Jong,[68] it seems that for a good efficiency, cross-over should be extremely likely in the population (a probability from 0.6 to 1) while mutation very unlikely (~ 0.001) and inversely proportional to the size of the population, the latter being moderately numerous.

Finally, let us stress that genetic algorithms are, by construction, very good at finding the neighborhood of the global minimum. But its exact position will generally not be found. Hence, it must be followed, in the final step of the search cycle, by a local optimization process.[69]

4.4.4 Neural networks

Neural networks follow an entirely different approach. Actually, a neural network consists in a set of processing elements called nodes whose functioning is loosely based on that of the neurons in the brain, hence the name. These nodes are interconnected in a network that can identify patterns in data without an *a priori* knowledge of causal relationships.[70] The important features of these neural networks is that they can learn, both from teaching and experience, and that their architecture is fundamentally parallel. The nodes are organized into layers. In a given layer, each node receives all the input generated by the previous layer. Each input value is then weighted and the weighted sum is compared to the threshold value of the node. The output value is set to 0 or to 1 depending on how they compare. The value of the weights and threshold is the basic characteristic of each node. The learning process consist in adjusting these

values to obtain a more correct output. This means that a neural network has to be trained before it is able to perform a certain task, as the characteristic values of each node have to be selected at random at the beginning. This training is done by repeatedly giving the network available data related to the problem so that, using the learning algorithm, it adjusts the various weights (and/or thresholds) to predict the correct output. Then, when presented with an unknown case, the neural network should be able to interpolate between the known cases, and even to extrapolate beyond them.

This approach has not been used yet to determine structures with electron spectroscopies (but it was successful to identify magnetic domain patterns[71]), but preliminary tests[2] seem to indicate that the learning process can be very time-consuming. It is nevertheless an approach that needs further consideration, especially as many different learning rules can be incorporated into a neural network. In particular, it is possible to use the genetic algorithm as the learning rule of a neural network. In this case, the weights and thresholds of all the nodes for a given configuration of the neural network are assembled to form a binary string, and a population of these strings is made to evolve according to the genetic algorithm rules.

5 Examples

We give here two brief examples of crystal structures solved by means of the methodology reviewed in the previous section. Both concern crystallographic information, one using scanned-energy PhD and the second with LEED.

5.1 Benzene/NO coadsorption on Ni(111)[72]

The problem here was to find the geometry of coadsorption of benzene and NO on a (111) surface of nickel. The PhD experiments were performed in the scanned-energy mode using a backscattering geometry, *i. e.* by exciting core levels of the adsorbate species. The nominal coverage was of 0.083 ML for benzene and of 0.167 ML for NO to obtain an ordered phase believed to contain one benzene and two NO molecules per unit mesh on the surface. No detailed structure information was available on this system although some was for the adsorption of one of the two species alone. The possible adsorption sites for benzene are sketched in Fig.8, together with the azimuthal directions in which the PhD data were collected. For NO, the two likely positions are a hexagonal compact hollow site (hcp) or a face centered cubic hollow site (fcc). Bao and coworkers[72] first inverted the experimental data using the projection method to obtain a good approximation of the structure to use as an input for the multiple scattering calculations. This inversion gave a strong probability of finding a N atom of NO located in a hcp hollow site approximately 0.13 nm above the surface Ni atoms. For benzene, the projection method did not give much information as it could not discriminate between the various possibilities shown in Fig.8: in every case the benzene molecule lies flat on the surface and the method sums up the contribution from all inequivalent C atoms. But earlier studies on pure benzene adsorption on Ni(111) seemed to favour a bridge-b position. Then, multiple scattering calculations were performed, starting from this trial structure and from the other possibilities sketched in Fig.8, using a linear approximation when necessary and a local multiparameter search around these trial structures. In this way, up to six parameters could be varied in the calculations. We give in Fig.9 the best fit simulations together with the experimental data. As can be seen, the agreement is very good. This unambiguously allowed to determine that the coadsorption took place in bridge-b position for benzene and hcp hollow site for NO. Furthermore, this study showed by a quantitative fitting of the internal and the external geometry of the benzene molecule that this molecule was not affected by the presence of NO. By contrast, the adsorbed benzene seems to produce some extension of the N-O bondlength of the order of 0.08 nm. The distance of N to the Ni surface was eventually found to be 0.115 nm which shows that the projection method had given it with a good approximation.

5.2 Adsorption of CO on Pd(111)[73]

This second example concerns LEED, but we show it here to illustrate the refining of a structure by the conjugate use of a tensor approximation and of a search method. The case is taken from Rous and coworkers[73]. It is simpler than the previous one as the only purpose was to improve the accuracy on the structural parameters of the already known case of CO on Pd (111). The start-

ing structure as described in the literature is shown in Fig.10 at the top left position. Then, the repeated use of Tensor LEED together with a local optimization algorithm for three parameters (expansion of the Pd top layer, adsorption height, CO bond length) produced the optimized structure in the top right position. The changes are significant and these results could only be achieved thanks to the tremendous gain of speed due to the use of the tensor approach (for small variations which is the case here), and the systematic exploration of the parameter space around the trial structure performed by the search algorithm. Another interesting point can be seen in the lower part of the figure where the evolution of the three structural parameters is plotted as a function of the steps in the search algorithm. We clearly see that there is a rapid convergence due to the fact that we explore only the region of the global minimum. But it is noteworthy that the convergence is imperative here because, although the *R*-factor decreases steadily with the advancement of the automated search, the structural parameters oscillate with it and their oscillations do not coincide.

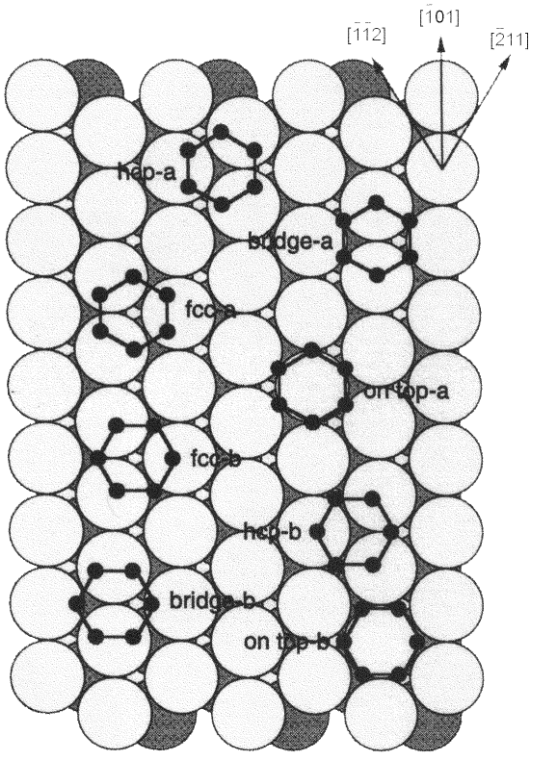

Fig.8 Plan view of the Ni(111) surface defining the principal azimuths in which PhD data were collected and also illustrating the possible local adsorption geometries for benzene molecules.[72]

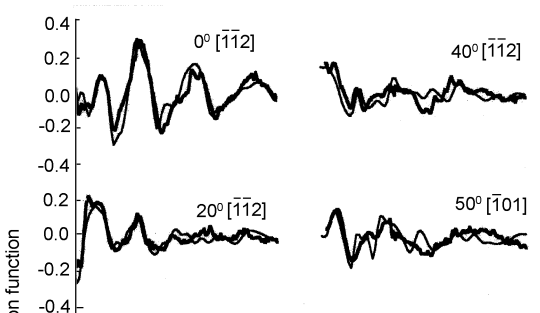

Fig.9 Comparison of the experimental C 1s PhD spectra (bold lines) with the best-fit theoretical simulations (fine lines).[72]

6 Conclusion

We have given here an overview of electron spectroscopies, both from a descriptive and practical point of view. These spectroscopies, in which an electron gathers the information, can be used from the mesoscale to the atomic scale to determine the crystallographic, electronic and magnetic structure of materials and of their surfaces. In the atomic scale case, they are one of the most accurate tools we possess for this purpose. But this accuracy can only be achieved through the systematic comparison to sophisticated calculations based on an adequate model. This part of the determination can become very time-consuming and hazardous, and therefore, we have shown how a strict methodology has to be followed in order to be successful. To be efficient, this methodology needs dedicated tools such as inverse methods, linearization schemes and search algorithms. All these tools, which we have critically assessed, are now well established which makes structure determination a routine task now for many materials. However, it should be noted that the ever increasing complexity of the materials that are studied now with these techniques, including proteins, imposes a new step in the development of the theoretical models to increase their rapidity if the actual accuracy is to be preserved or improved.

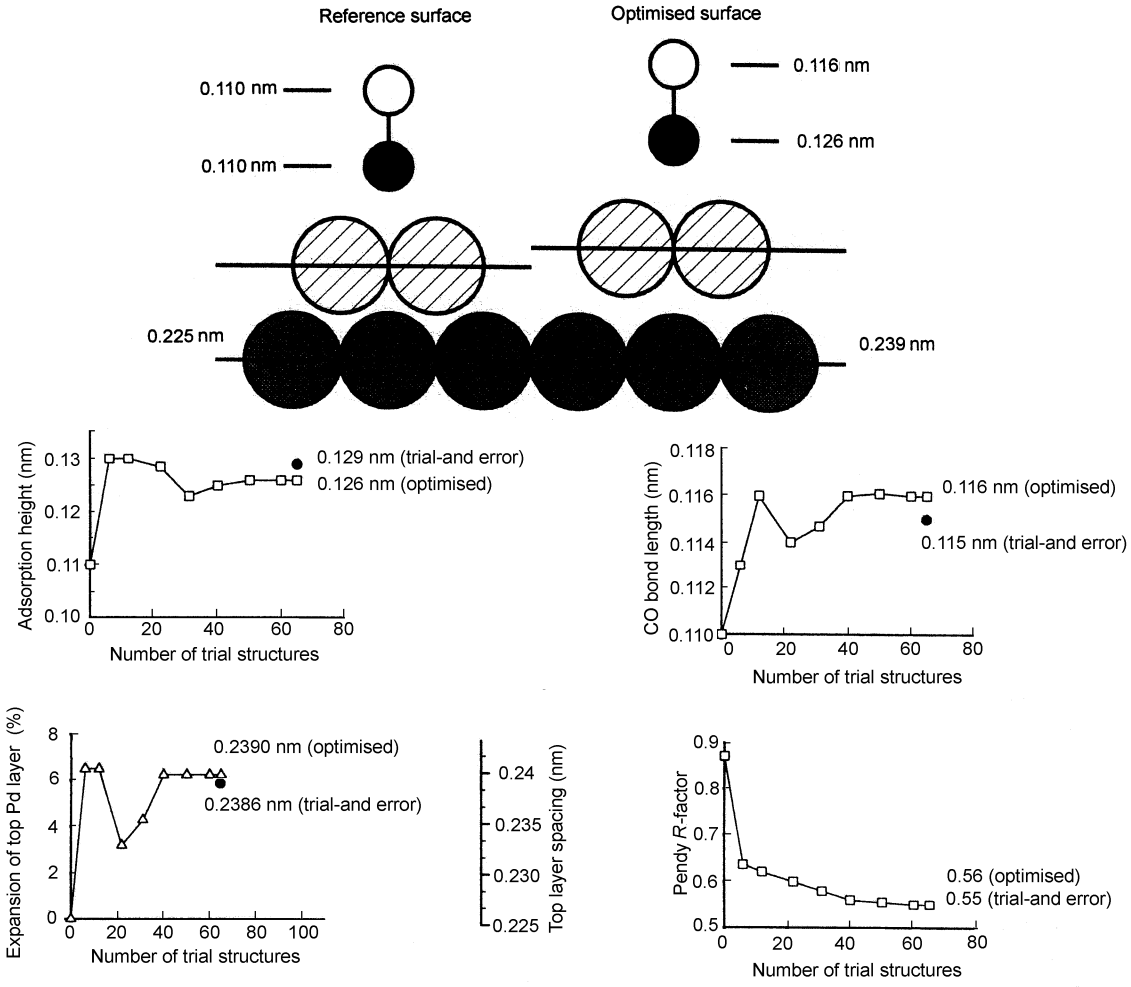

Fig.10 Top: structural model of $c(4\times2)$-CO/Pd(111) with structural parameters given for the reference (left) and optimized (right) structure. Bottom: progress of the directed search using Tensor LEED for the above structure as a function of the number of iterations.[73]

Acknoledgments

We are grateful to Francine Solal for a critical reading of the manuscript and for helpful comments. Zi-Yu WU acknowledges the financial support of the 100-Talent Research Program of the Chinese Academy of Sciences and of the Outstanding Youth Fund (10125523) and Key Important Nano-Research Project (90206032) of the National Natural Science Foundation of China.

References

1 Surface science. The first thirty years, Duke C B editor, North-Holland, 1994

2 Van Hove M A, Surf Interface Anal, 1999, **28**: 36

3 Watson P R, Van Hove M A, Hermann K. NIST Surface Structure Data Program Ver. 2.0, NIST Standard Reference Data Program, Gaithersburg, MD, USA, 1996

4 Osterwalder J, Aebi P, Photoelectron diffraction and Fermi surface mapping, World Scientific, 2003

5 Woodruff D P, Delchar T A, Modern techniques of surface science, second edition, Cambridge University Press, 1994

6 Somorjai G A, Introduction to surface chemistry and catalysis, Wiley-Intersciences, 1994

7 Niemantsverdriet J W, Spectroscopy in catalysis-An introduction, VCH, 1995

8 Flewitt P E J, Wild R K. Physical methods for materials characterisation, Institute of Physics Publishing, 1994

9 Pendry J B, Low energy electron diffraction, Academic Press, 1974

10 Van Hove M A, Tong S Y. Surface crystallography by LEED, Springer Verlag, 1979

11 Van Hove M A, Weinberg W H, Chan C M. Low-energy

electron diffraction, Springer Verlag, 1986
12 Heinz K. Phys Stat Sol, 1994, **A146**: 195
13 Heinz K. Rep Prog Phys, 1995, **58**: 637
14 X-ray absorption, Königsberger D K , Prins R editors, Wiley, 1987
15 Lee P A, Citrin P H, Eisenberger P *et al.* Rev Mod Phys, 1981, **54**: 769
16 Stöhr J. NEXAFS spectroscopy, Springer Verlag, 1992
17 X-ray absorption: principles, applications, techniques of EXAFS, SEXAFS and XANES, Königsberger D K, Prins R editors, 1988
18 Thole B T, Carra P, Sette F *et al.* Phys Rev Lett, 1992, **68**: 1943
19 Fadley C S. Advances in surface and interface science, Bachrach R Z editor, Plenum Press, 1992, 421
20 Fadley C S, Van Hove M A, Hussain Z. Surf Rev Lett, 1997, **4**: 421
21 Fadley C S. Prog Surf Sci, 1997, **54**: 341
22 Kostroun V O, Chen M H, Craseman B. Phys Rev, 1971, A**3**: 533
23 Raether H. Springer tracts in modern physics, **88,** Springer Verlag, 1980
24 Thiry P A, Liehr M, Pireaux J J *et al*. Physica Scripta, 1987, **35**: 368
25 De Crescenzi M, Antonangeli F, Bellini C *et al*. Phys Rev Lett, 1983, **50**: 1949
26 Caputi L S, Comite O, Amoddeo A *et al*. Phys Rev Lett, 1996, **77**: 1059
27 De Crescenzi M, Lozzi L, Picozzi P *et al*. Phys Rev, 1989, **B39**: 8409
28 Sébilleau D. Surf Sci, 2001, **482/485**: 729
29 Šimunek A, Vackář J, Sobczak E. Phys Rev, 1988, **B38**: 8515
30 Šimunek A, Sipr O, Vackář J. Phys Rev Lett, 1989, **63**: 2076
31 Šipr O, Vackář J, Šimunek A. Phys Rev, 1991, **B44**: 4832
32 Sébilleau D. submitted to Phys Rev B
33 Natoli C R. Physica, 1995, **B208/209**: 5
34 Sébilleau D. Phys Rev, 2000, **B61**: 14167
35 Faddeev L D. Mathematical aspects of the three-body problem in the quantum scattering theory, Israel program for scientific translation, 1965
36 Faulkner J S, Stocks G M. Phys Rev, 1980, **B21**: 3222
37 Sayers D E, Stern E A, Lytle F W. Phys Rev Lett, 1971, **27**: 1204
38 Barton J J, Bahr C C, Hussain Z *et al*. Phys Rev Lett, 1983, **51**: 272
39 Fritzsche V, Woodruff D P. Phys Rev, 1992, **B46**: 16128
40 Schindler K M, Hofmann Ph, Fritzsche V *et al*. Phys Rev Lett, 1993, **71**: 2054
41 Hofmann Ph, Schindler K M, Bao S *et al*. Nature, 1994, **368**: 131
42 Schaff O, Hofmann Ph, Hirschmugl C J *et al*. J Electron Spec Relat Phenom, 1995, **76**: 85
43 Szöke A Short wavelength coherent radiation: generation and application, Atwood D T, Boker J editors, AIP Conf Proc No. 147, AIP, 1986
44 Barton J J. Phys Rev Lett, 1988, **61**: 1356
45 Hu P, King D K. Nature, 1992, **360**: 655
46 Saldin D K, de Andres P L. Phys Rev Lett, 1990, **64**: 1270
47 Kopecky M, Lausi A, Busetto E *et al*. Phys Rev Lett, 2002, **88**: 185503
48 Len P M, Zhang F, Thevuthasan S *et al.* J Electron Spec Relat Phenom, 1997, **85**: 145
49 Tonner B P, Han Z L, Harp G R *et al.* Phys Rev, 1991, **B43**: 14423
50 Tong S Y, Wei C M, Zhao T C *et al*. Phys Rev Lett, 1991, **66**: 60
51 Wu H, Lapeyre J D. Phys Rev, 1995, **B51**: 14549
52 Wider J, Baumberger F, Sambi M *et al*. Phys Rev Lett, 2001, **86**: 2337
53 Omori S, Nihei Y, Rotenberg E *et al*. Phys Rev Lett, 2002, **88**: 055504
54 Daimon H, Imada S, Suga S. Surf Sci, 2001, **471**: 143
55 Saldin D K, Harp G R, Chen B L *et al*. Phys Rev, 1991, **B44**: 2480
56 Lee P A, Pendry J B. Phys Rev, 1975, **B11**: 2795
57 Ashley C A, Doniach S. Phys Rev, 1975, **B11**: 1279
58 Fujikawa T. J Phys Soc Jpn, 1982, **51**: 251
59 Barton J J, Shirley D A. Phys Rev, 1985, **A32**: 1019
60 Gavaza M, Sébilleau D. Surf Sci, in press, 2003
61 Rous P J, Pendry J B, Saldin D K *et al.* Phys Rev Lett, 1986, **57**: 2951
62 Wander A, Pendry J B, Van Hove M A. Phys Rev, 1992, **B46**: 9897
63 Fritzsche V, Pendry J B. Phys Rev, 1993, **B48**: 9054
64 Kaduwela A P, Van Hove M A, Fadley C S. Surf Sci, 1994, **302**: L336
65 Zanazzi E, Jona F. Surf Sci, 1997, **62**: 61
66 Ynzunza R X, Tober E D, Palomares F J. Surf Sci, 1999, **441**: 301
67 Döll R, Van Hove M A. Surf Sci, 1996, **355**: L393
68 De Jong K A. Foundations of genetic algorithms 2, Whitley L D editor, Morgan Kaufmann Publishers, 1993

69 Dane A D, Veldhuis A, de Boer D K G *et al*. Physica, 1998, **B253**: 254

70 Beale R, Jackson T. Neural computing: an introduction, Adam Hilger, 1990

71 Courtin S, Padovani S. Europhys Lett, 2000, **50**: 94

72 Bao S, Lindsay R, Polcik M *et al*. Surf Sci, 2001, **478**: 35

73 Rous P J, Van Hove M A, Somorjai G A, Surf Sci, 1990, **226**: 15